

On the accretion flow and mass accretion rates/fluctuations in black hole candidate; MAXI J1535–571

Ambrose C. Eze^{a,*}, Romanus N.C. Eze^b, Augustine E. Chukwude^b, Fidelis O. Madu^a

^a Department of Physics and Geosciences, Faculty of Natural Sciences and Environmental Studies, Godfrey Okoye University, Enugu, Nigeria

^b Department of Physics and Astronomy, Faculty of Physical Sciences, University of Nigeria, Nsukka, Nigeria

ARTICLE INFO

Keywords:

Transient source
Black hole candidate
MAXI J1535–571-out-burst evolution
Accretion flow-mass accretion rates
X-ray emissions
Variations/fluctuations

ABSTRACT

MAXI J1535–571 underwent dramatic and transient outbursts accompanied by accretion flow. Hard X-radiations are produced due to thermal–and inverse–comptonization of soft photons by high-temperature electrons. The variations/fluctuations of components of the accretion flow rates and their fractional X-ray emissions/flux variability contributions at different epochs infer the spectral states. In this study, we utilized MAXI J1535–571 data observed by the three X-ray missions/detectors (MAXI/GSC, NuSTAR, and SWIFT/BAT) on the same and/or close-in epochs. Each detector's data were separately reduced and analyzed using HEASoft v6.28 and its software packages alongside the standard pipeline product software of each detector. Thereafter, the MAXI J1535–571 data were simultaneously fitted in XSPEC version 12.10.1f and modelled using selected analytical and phenomenological models (AP-model) to examine the photon index– N_{BMC} saturation effect and variations of components of the accretion flow rates. Moreover, the TCAF model was used on MAXI J1535–571 data to determine the correlation of components of the accretion flow rates. The AP- and TCAF-models gave a statistically acceptable fit with a reduced Chi-squared value of ≤ 1.2 , and their spectral results were compared. The best-fit photon index of ~ 2.0 – 2.20 affirms that MAXI J1535–571 is in its rising phase; the hard-intermediate state. The correlation of mass accretion rates suggests that their variations/fluctuations could be responsible for the dynamics and geometry of the accretion flow.

1.0. Introduction

Low Mass X-ray Black Hole Binaries (LMXBHBs) are a compact binary system that contains a black hole and a donor star. Black holes grow in mass due to gravitation and magneto-hydrodynamic processes. The ejecting particles from the inner Lagrange point of the donor star accumulate around the black hole via Roche lobe overflow mechanisms. This enriches the black hole alongside the formation of an accretion disk on timescales. When the mass accretion rate of the black hole approaches that of the Eddington limit, centrifugal-, radiation pressure-, and magneto-rotational-processes initiate and mediate accretion-ejection coupling. This creates shear-driven turbulence that stirs up the accretion disk. As a result, rapid instabilities and enhanced viscosity on large length scales trigger an outburst, and the accretion flow (outflow matter) is driven by advection, radiative, and hydrodynamic processes [1–9]. The accretion flow consists of optically thick- and optically thin- plasma according to the truncated disk model. This

plasma explains the thermal (multi-temperature black body) and power-law (non-thermal or comptonized) component radiations originating from the accretion disk and Compton cloud/corona respectively [10,11]. In the same vein, the TCAF model assumes that Keplerian flow and sub-Keplerian flow are the components of the accretion flow that explain the thermal (soft) and power-law/comptonized radiations respectively [12,13]. The significance of both models is that hard X-rays are produced when soft photons are thermally or inverse comptonized by high-temperature electrons, but their mechanisms differ. The truncated disk model assumes that the accretion disk is truncated outside the innermost stable circular orbit (ISCO) and the hot, radiatively inefficient optically thin plasma develops inside it. On the other hand, the TCAF model assumes CENBOL (CENTrifugal pressure supported BOUNDary Layer) with the Keplerian flow sandwiched in between the sub-Keplerian flow, and the emerging soft photons are conveyed to the sub-Keplerian (post-shock) region via magnetic activities and buoyancy [10,14–18]. The gradual manifestation of the soft photons in the

* Correspondence author.

E-mail addresses: ceze@gouni.edu.ng (A.C. Eze), romanus.eze@unn.edu.ng (R.N.C. Eze), augustine.chukwude@unn.edu.ng (A.E. Chukwude), madufidelis@gouni.edu.ng (F.O. Madu).

<https://doi.org/10.1016/j.astropartphys.2024.103076>

Received 11 June 2024; Received in revised form 17 November 2024; Accepted 20 December 2024

Available online 24 December 2024

0927-6505/© 2024 Elsevier B.V. All rights are reserved, including those for text and data mining, AI training, and similar technologies.

post-shock region (Compton cloud/corona), as the outburst progresses, dilutes the heating process and mediate cooling [12,19–21]. This leads to a decrease in the size/height alongside the temperature of the post-shock region as well as softening of the hardness of the X-ray spectrum and spectral states [13,19,22]. Four spectral states (hard state; HS, hard-intermediate state; HIMS, soft-intermediate state; SIMS, and soft state; SS) have been identified [7,23–25]. These spectral states are regulated by the evolution of accretion flow properties {mass accretion rate (\dot{M}), photon index (Γ), temperature, luminosity, etc.; [20,26–28]}. The energy radiated during the outburst evolution/spectral states is an indication of stored mass on timescales (\dot{M}) during quiescence [29]. Besides, the X-ray flux variability of BHCs is strongly linked to the mass accretion rate variations/fluctuations [7,11,17,23,30,31]. Moreover, the power-law photon index (Γ) varies from lower to higher values during the hard-to-soft spectral state transition and tends to saturate with an increase in the normalization parameter of the *bmc* model (N_{bmc} : which is directly proportional to optically thick (disk) flow mass accretion rate; [21,32,33]). The Γ – N_{bmc} track varies for different sources and even for the same source at different epochs [34]. The traces of convergent flow are observed not only in the soft states (SS and SIMS), but also in the HIMS and HS [12]. Hence, the saturation effect, X-ray flux variability, and spectral states are tied to the accretion flow properties. Probing the spectral properties of BHCs during their outburst evolution could give clues on the structure, dynamics, and geometry of accretion flow on timescales.

1.1. Outburst evolution of MAXI J1535–571

MAXI J1535–571 outburst was detected on September 02, 2017 (MJD58001; [35]) in the constellation Norma by Monitor of All-sky X-ray Image satellite (MAXI/GSC; [36]). *Swift/BAT* (Swift/Burst Alert Telescope) followed suit in observing it on September 5, 2017 [37]. Moreover, Nuclear Spectroscopic Telescope Array (*NuSTAR*) co-observed MAXI J1535–571 on September 7, 2017 (MJD 58,003; [38]), and multi-wavelength observations have also been reported [8, 39,40]. MAXI J1535–571 distance of 4.5–6.5 kpcs in the Galactic center at RA; $15^{\text{h}} 35^{\text{m}} 19.73^{\text{s}}$ and Dec; $-57^{\circ} 13' 48''$ respectively have been constrained [41,42]. The onset of the outburst was dramatic with an average hard X-ray flux of $1.25 \times 10^{-9} \text{ erg cm}^{-2} \text{ s}^{-1}$ which rapidly increased to $5.3 \times 10^{-8} \text{ erg cm}^{-2} \text{ s}^{-1}$ and later attained $12 \times 10^{-8} \text{ erg cm}^{-2} \text{ s}^{-1}$ in the 2–20 keV energy bands [43]. This happened between September 02–10, 2017 and these epochs indicate the hard spectral state. MAXI J1535–57 moved to the hard-intermediate state (HIMS) on September 12, 2017, and stayed in this epoch till September 18, 2017, before it moved to the soft-intermediate (SIMS) on September 19 to 24, 2017. Thereafter, MAXI J1535–57 exhibited soft spectral (SS) characteristics on January 19, 2018 [43,44]. The hard-to-soft spectral transition is accompanied by an increase in the power-law photon index. A photon index of ~ 1.97 to 2.3 indicates that MAXI J1535–57 is in the intermediate spectral state [43–45]. Also, a “short-lived” intermittent/flickering behavior accompanied by enhanced magnetic and re-flares activities has been seen in the intermediate state [38,42,46], but the physical mechanism(s) responsible for the MAXI J1535–571’s flickering behavior, X-ray flux variability, dynamics, and geometry of the accretion flow is ongoing.

In this paper, spectral analysis of MAXI J1535–571 was carried out to explain the physical mechanism responsible for the saturation effect in the accretion flow characteristics and determine the variations/fluctuations of mass accretion flow rates. Section 2 describes the data acquisition and reduction. Spectral analysis/fitting and modelling techniques and results are presented in section 3. The discussion and conclusion are presented in Section 4. Moreover, it is worth noting that we are submitting another manuscript/paper on spectral analysis of MAXI J1535–571 dataset observed on September 14, 2017, to elucidate the saturation effect, track/anti-correlation of components of the accretion flow rates and other accretion flow characteristics with one another,

dynamic of the accretion flow, and explains the origin of power-law photon index–Quasi-Periodic Oscillation frequency (Γ –vQPO) relation, and intermittent/flickering behavior of the accretion flow.

2. DATA acquisition and reduction

This study utilized two simultaneous *MAXI/GSC*, *SWIFT/BAT*, and *NuSTAR* datasets on September 14, 2017, when the source was in the hard-intermediate state [43,44]. On this day, *NuSTAR* performed two observations with exposures of ~ 2 ks starting from UT 05:11:09 and 13:16:09 which end at UT 09:51:09 and 20:16:09 (OBSIDs; 80,402,302, 002 and 80,402,302,004) respectively. Hereafter, we call these two epochs as Epoch-A and Epoch-B respectively. We downloaded the *NuSTAR* data from the HEASARC archive¹ and reprocessed them using the standard pipeline tool *nupipeline* version 1.6 with the *NuSTAR* CALDB version 20,170,817. The time-averaged spectra and their response files were made for the individual OBSIDs using *nuproducts* included in HEASoft version 6.26.1. Here the source extraction region was defined as a circle with 80 arc-minutes centered at the source position. The background region was defined as 100 '' in a source-free area. We also used the *MAXI/GSC* and *Swift/BAT* data overlapping the two *NuSTAR* observations. For the *MAXI/GSC*, we obtained the time-averaged spectra from UT 03:36:00 to 06:00:00 for Epoch-A and from UT 17:35:59 to 19:59:59 for Epoch-B through the *ondemand* web interface². The source events were extracted from a circular region with an 80 arc-minute radius which covers about 90 % of the source’s flux. The background spectrum extraction was made in a blank-sky area near the source region using a circular region of 150 arc-minute radius. For the *Swift/BAT*, we downloaded the survey-mode data starting from UT 05:02:51 and 14:23:29 to 5:21:58 and 14:41:58 for Epoch-A and Epoch-B respectively from the HEASARC archive and reduced with the *Swift/BAT* CALDB released on 2017 October 16. We reduced the data with the HEASoft FTOOL *batsurvey* and created the time-averaged spectra and the response files with the dedicated script *make_survey_pha* from the *batsurvey* products.

3.0. Spectral analysis and results

3.1. Spectral analysis

The spectral analysis was done using *XSPEC* version 12.10.1f. A combination of analytical, phenomenological, and physical models [12, 21,27,30,47] was used to estimate the mass accretion flow rates and obtain their correlation. Modelling the X-ray spectrum of BHCs with the bulk motion comptonization (*bmc*) model reveals how soft photons of the accretion flow undergo thermal comptonization in the presence of hot electrons. The photon index ($\Gamma = \alpha + 1$, where α is the energy spectral index) and normalization parameter are linearly correlated, but Γ saturates with further increase in normalization parameter [48,49]. This correlation gives clues to spectral states [33]. Modelling the spectral states (HS, HIMS, SIMS, SS) of BHCs with the *bmc* model alongside a *Gaussian* model and other *XSPEC* models gives a good statistical spectral fit [50,51]. The temperature (T_i) of the optically thick flow/plasma where the X-ray soft photons are produced is [27];

$$T_i = \left[\frac{3GM_{\odot} \dot{M}_{\text{op.thickflow}}}{8\pi\sigma_B r_i^3} \left(1 - \beta \sqrt{\frac{R_i}{r_i}} \right) \right]^{1/4}. \quad (1)$$

Where G , M , $\dot{M}_{\text{op.thickflow}}$, and σ_B is the gravitational constant, the mass of the black hole in the Solar unit, optically thick flow (accretion disk) mass accretion rate, and Stefan-Boltzmann constant ($5.6692 \times 10^{-5} \text{ erg cm}^{-2} \text{ K}^{-4} \text{ s}^{-1}$) respectively. The parameter β in Eq. (1) defines the

¹ <https://heasarc.gsfc.nasa.gov/docs/archive.htm>.

² <http://maxi.riken.jp/mxondem/>.

inner boundary condition of the disk. It is either 0 (non-relativistic approximation) or 1 (relativistic approximation). The “apparent” inner disk radius (r_i ; in kilometers) was estimated from the normalization (k) parameter of the *diskbb* [52];

$$r_i = \left(\frac{\kappa}{\cos\theta} \right)^{1/2} \times D, \quad (2)$$

where D is the distance of the source in kpc, and θ is the angle of inclination of the system.

The real radius (R_i) of the optically thick flow/plasma was obtained by introducing a correction factor (ξ ; [27]);

$$R_i = \xi \cdot K^2 \cdot r_i, \quad (3)$$

where K is the hardening factor [a ratio of color temperature to an effective temperature (1.7 – 2.0)] and $\xi = \sqrt{3/7 \times (6/7)^3} = 0.5 \simeq 1$ [48,53]. We adopted relativistic approximation ($\beta = 1$) and substituted eqn. (3) into eqn. (1);

$$T_{max}^4 = \frac{3GM_{\odot} \dot{M}_{op.thickflow}}{8\pi\sigma_B r_i^3} \left(1 - \sqrt{\xi \cdot K^2} \right). \quad (4)$$

The X-ray luminosity and mass accretion rate of the optically thick flow are related as follows;

$$L_{op.thickflow} = \frac{3GM_{\odot} \dot{M}_{op.thickflow}}{2R_i} \times \left(1 - \sqrt{\xi \cdot K^2} \right). \quad (5)$$

The X-ray flux of the optically thick flow/plasma is;

$$F_{op.thickflow} = \frac{L_{op.thickflow} \times \cos\theta}{2\pi D^2} \quad (6)$$

The X-ray flux of the accretion flow is the $F_{op.thickflow}$ plus X-ray flux of the optically thin flow ($F_{op.thinflow}$); [10,54];

$$F_{op.thickflow} + F_{op.thinflow} 2\cos\theta = 0.0165 \left[\frac{r_i^2 \cos\theta}{(D/10kpc)^2} \right] \left(\frac{T_i}{1keV} \right)^3 \times photons^{-1} cm^{-2}. \quad (7)$$

The X-ray emission from the optically thin flow is isotropic and thermally Comptonized with luminosity;

$$L_{op.thinflow} = 4\pi D^2 F_{op.thinflow}, \quad (8)$$

where the $F_{op.thinflow}$ is the X-ray flux (in the corona due to scattered photons) and D is the distance of the source. The mass accretion rate of the optically thin flow/corona is [54];

$$\dot{M}_{op.thinflow} = \frac{L_{op.thinflow}}{\eta c^2}, \quad (9)$$

where c , η , and $L_{op.thinflow}$ is the velocity of light, radiative coefficient flow, and luminosity of the optically thin flow/plasma respectively. The value of radiative efficiency flow (η) ranges from 0.001 to 1. For a non-rotating black hole, $\eta = 0.8$ is assumed since its value is much greater than 0.1 for radiatively inefficient flow/plasma [54]. Moreover, the mass accretion flow rates [Keplerian (disk; m_{dotd}) and sub-Keplerian (halo; m_{dotoh})] of MAXI J1535–571 can be constrained directly using the physical (TCAF) model. Moreover, TCAF model gives the following accretion flow properties; (i) compression ratio ($R = \rho^+ / \rho^-$; ρ^+ & ρ^- is the density of the post-shock and pre-shock matter respectively), (ii) mass of the black hole (M_{bh}) in the Solar unit, (iii) location of the shock (X_s in units of Schwarzschild radius; $r_g = 2GM_{bh} / c^2$), and (iv) norm (equivalent to $(4\pi D^2)^{-1} \times \cos(\theta)$; where $\theta =$ angle of inclination, and $D =$ distance of the source in kpc) respectively [55–57].

While fitting the MAXI J1535–571 Epoch-A and Epoch-B data, the energy bands where there is a low signal-to-noise ratio were ignored using the XSPEC *ignore command*. In Epoch-A, data within 15–140 keV,

3.2–79 keV, and 3.2–20 keV bands were used for *Swift/BAT*, *NuSTAR*, and *MAXI/GSC* detectors respectively. In the same vein, data within 15–100 keV, 2.0–13 keV, and 3.0–40 keV bands were used in Epoch-B for *Swift/BAT*, *MAXI/GSC*, and *NuSTAR* detectors respectively. To take account of the X-ray spectrum absorption by neutral material and instrumental artifacts, the multiplicative “*tbabs*” [58] and cross-calibration constant (*const*) energy-independent components were used. The Epoch-A data were first fitted/modelled using *const*tbabs*(bmc)*. This gives a very high reduced Chi-squared value of 6.85 (191.86/28). This is above the acceptable limit, and as a result, the spectral fitting was re-normalized and modelled again using *const*tbabs*(bmc*highcut)*. This gives a reduced Chi-squared value of 2.295 (59.66/26). The F-statistic test was performed to determine the significance of the high energy cutoff model, and an F-test/probability value of $28.806/2.541 \times 10^{-7}$ was obtained. The *highcut* (high energy cutoff) model gives the cutoff energy and e-fold energy of the electron in keV.

The *diskbb* model was added to explain the multi-black body component radiations and to constrain the true radius and temperature of the accretion disk/optically thick flow/plasma [59]. This did not significantly improve the fit statistic with an F-test/probability value of 1.215/0.332 and a reduced Chi-squared of 2.220 (48.86/22). The *diskbb* model is associated with gross formalism and this was corrected by adding the *grad* (general relativistic accretion disk model; [60]). The fit statistic did not improve as such with an F-test/probability of 1.156/0.294 and a reduced Chi-squared of 2.205 (46.31/ 21). Though the *diskbb* or *grad* model explains the thermal components of X-radiations originating from the accretion disk, another reason for adding the *grad* model was to constrain the spectral fit parameters (mass of the black hole, distance and inclination angle of the source, mass accretion rate of the optically thick flow, and spectral hardening factor). Later, a Gaussian (*gaus*) model was added to explain the reflection component of the accretion flow. This improved the fit statistic with a reduced Chi-squared value of 1.88 (30.10/16) and an F-test/probability of 1.723/0.186. The inclination angle and distance of the source were “thawed” and “stepped” from 4.5 kpc to 6.5 kpc and 45° to 60° respectively to see if the fit statistic would improve, and later a systematic error of 2 % was used. This gives an acceptable reduced Chi-squared value of 1.246 (18.70/15) with an F-test/probability value of $9.144/8.54 \times 10^{-3}$. The composite model is *const*tbabs*(bmc*highcut+diskbb+grad+gaus*; hereafter AP-model). To ascertain the consistent value of the photon index, we modeled the Epoch-A data again with *const*tbabs*(PL+diskbb)*, and a photon index value of 2.1 was obtained. The *PL* is a cold matter power-law absorption model that explain the X-ray transmission and Compton scattering of soft photons around an isotropic source [61]. The *PL* model gives the power-law photon index, absorption column density and other parameters.

The photon index–normalization parameter (Γ – N_{bmc}) track characteristics were obtained using the *bmc* model’s-fitted parameters. We assumed relativistic approximation ($\beta = 1$), and utilized the *diskbb* and *grad* model’s-fitted parameters in MATLAB written codes of physical Eqs. (2–9) to estimate the optically thin flow/plasma mass accretion rates. The radius of the optically thick flow was estimated from the normalization (k) of *diskbb* using Eqn. (2 & 3). It is worth noting that R_i is a little boost of r_i . Whether R_i or r_i is substituted in Eq. (5) shows no significant change in value of $L_{op.thickflow}$. This could be probably a close-in epoch observed data were used. As a result, using R_i to represent the true inner radius of the optically thick flow where the seed soft photons originate is not bad. The inclination angle (58°), distance (6.5 kpc), and mass of the black hole ($9.8 M_{\odot}$) employed in Eqn. (2) were constrained from *grad* model. The luminosity of the optically thick flow was estimated using Eqn. (5). The optically thick flow mass accretion rate ($\dot{M}_{op.thickflow}$) and hardness factor (K) value of 1.7 employed in Eqn. (5) were constrained from the *grad* model. Eqn. (6) was used to estimate the X-ray flux of the optically thick flow. Eqs. (7), (8), and (9) were used to estimate the X-ray flux, luminosity, and mass accretion rate of the optically thin flow ($\dot{M}_{op.thinflow}$) respectively. The units of optically thick flow

mass accretion rate ($\dot{M}_{\text{op,thickflow}}$) and optically thin mass accretion rate ($\dot{M}_{\text{op,thinflow}}$) is in kilograms/second. Moreover, the Epoch–A data was modelled with *const*tbabs* alongside the *TCAF* model [*const*tbabs*(TCAF_v0.3.2.R1)*] to constrain the Keplerian flow (m_{dotd}), and sub-Keplerian flow (m_{doh}) mass accretion rates (in Eddington limit), and the mass of the black hole (M_{bh}). This gives a reduced Chi-squared value of 1.338 (24.09/18). Thereafter, a *Gaussian* model was added to account for the reflection components of the accretion flow. This improved the fit statistic with a reduced Chi-squared value of 1.108 (17.73/16) and an F-test/probability value of 2.86/0.086. While fitting, m_{dotd} and m_{doh} were linear “steppar” to run 80 iterations, and their contour plot was obtained. For Epoch–B, we repeated the same techniques of fitting/modelling as in Epoch–A. Modelling the Epoch–B data using *const*tbabs*(bmc)* gives an unacceptable reduced Chi-squared value of 2.25 (1090.91/ 484). The fitting was re-normalized and the data was modelled again using *const*tbabs*(bmc*highcut)*. The fit statistic improved with a reduced Chi-squared value of 1.56 (752.10/482) and an F-test/probability value of 108.567/1.18929 $\times 10^{-39}$. The *diskbb* model was added and the fit statistic improved with a reduced Chi-squared value of 1.1087 (532.15/480) and an F-test/probability value of 99.197/8.750 $\times 10^{-37}$. Subsequently, the *grad* and *gaus* model were added one after the other. These improved the fit statistic with a reduced Chi-squared value of 1.085 (515.82/475) and 1.0269 (484.69/472) alongside an F-test/probability value of 31.0831/1.91096 $\times 10^{-35}$ and 10.105/1.834 $\times 10^{-06}$ respectively. Thereafter, the consistent value of the photon index was checked using *const*tbabs*(PL+diskbb)*, and a photon index value of 2.2 was obtained. The Γ - N_{bmc} correlation and the estimation of the optically thin flow and optically thick (disk) flow mass accretion rates for Epoch–B were determined using the same techniques employed in Epoch–A. Later, the fitting was re-normalized and modelled again using *const*tbabs*(TCAF_v0.3.2.R1)*. This gives a reduced Chi-squared value of 2.265 (1092.07/482). Adding a *Gaussian* model improved the fit statistic with a reduced Chi-squared value of 1.526 (731.01/ 479) and an F-test/probability value of 78.8625/1.790 $\times 10^{-41}$. The m_{dotd} and m_{doh} were linear “steppar” to run for 50 iterations and their contour plot was obtained. This gives a reduced Chi-squared value of 1.0817 (514.89/476) and an F-test/probability value of 66.598/5.665 $\times 10^{-36}$. However, we spotted in the Epoch–B X-ray spectrum residuals around 6–7 keV that the *MAXI/GSC* data (red) were not well fitted. Given this, the fitting was re-normalized and modelled again using reflection relativistic (*relxill*) models [62]. The data was modelled using *relxillCp* alongside *diskbb* [*const*tbabs*(diskbb+relxillCp)*]. This gives a photon index, spin parameter, reflection fraction, and electron temperature of 2.08, 0.99 (cJ GM²), 4.65, and 54.16 (keV) with a reduced Chi-squared value of 1.129 (534.01/ 473). Later, the *relxillCp* model was replaced with *relxillp* and modelled again. This gives a lamp-post height of 6.251 (GM/c²). These fittings/modellings were repeated for Epoch–A and consistent value of the aforementioned parameters were obtained. Though these models give a reduced Chi-squared value of ≤ 1.2 , there is no change or difference in the shape of the X-ray spectrum (fitted/modelled data and residuals) in comparison to that of the *AP*- and *TCAF* -models. Therefore, we present the X-ray spectra and spectral parameters of Epoch–A and Epoch–B obtained using the *AP*- and *TCAF*-models in Tables 1 & 2 because they reproduced the data well. The errors in each spectral fit parameter of Epoch–A and Epoch–B were obtained using *XSPEC error command*. The correlation of the model’s-fitted and estimated parameters was obtained using MATLAB, and Pearson correlation was used to determine the correlation coefficient.

3.2. Results

Tables 1 and 2 show the best fit spectral parameters of the *AP*-model and *TCAF*-model respectively. The errors in each spectral parameter are at a 90 % confidence limit. Table 3 shows the Pearson correlation coefficient of the parameters.

Table 1

Best fit spectral parameter of MAXI J1535–571 using *AP*- models.

Spectral Parameters	Epoch-A	Epoch-B	Unit
Constant factor	0.99 \pm 0.04	0.91 \pm 0.08	
N_{H}	(3.45 ^{+0.25} _{-0.16}) $\times 10^{22}$	(3.2 \pm 0.14) $\times 10^{22}$	cm ⁻²
kT _{Bmc}	1.43 ^{+0.20} _{-0.12}	1.197 ^{+0.621} _{-0.230}	keV
Γ ($\alpha + 1$) _{Bmc}	1.845 ^{+0.313} _{-0.014}	1.841 ^{+0.254} _{-0.140}	–
norm _{Bmc}	2.285 \pm 0.13	4.216 \pm 0.038	erg s ⁻¹ kpc ⁻²
Ec _{highcut}	26.201 ^{+0.101} _{-1.015}	32.102 ^{+0.052} _{-1.061}	keV
E _{fhighcut}	35.246 ^{+2.110} _{-0.210}	39.243 ^{+0.001} _{-0.092}	keV
T _{idiskbb}	1.412 ^{+0.713} _{-0.721}	1.802 ^{+0.052} _{-0.036}	keV
norm _{diskbb}	253.861 ^{+0.780} _{-0.103}	206.625 ^{+0.571} _{-0.021}	–
D _{grad}	6.531 ^{+0.031} _{-1.410}	6.49 \pm 0.18	kpc
Θ_{grad}	57.651 \pm 1.36	58.302 \pm 0.05	degree
M _{bhgrad}	9.835 ^{+0.248} _{-0.011}	10.013 \pm 0.09	M _⊙
M _{ddgrad}	(1.913 \pm 0.042) $\times 10^{18}$	(2.21 \pm 0.01) $\times 10^{18}$	grams/sec
hd _{grad}	1.701 \pm 0.201	1.68 \pm 0.07	–
norm _{grad}	65.0242 ^{+1.17} _{-0.98}	68.025 ^{+0.011} _{-0.705}	–
E _{6.5_gaus} (keV)	6.48 \pm 0.051	6.56 \pm 0.10	
sigma _{gaus} (keV)	3.14 \pm 0.431	0.279 \pm 0.07	
norm _{gaus}	0.55 \pm 0.081	1.86 \pm 0.02	
χ^2	19.70	484.69	–
d.o.f	16	472	–
R χ^2	1.231	1.026	–
NhP	2.34 $\times 10^{-01}$	3.33 $\times 10^{-01}$	–

KT_{Bmc} = Temperature of thermal photon of the source, $\Gamma(\alpha + 1)$ _{Bmc} = photon index (spectral index +1), norm_{Bmc} = absolute normalization of *bmc* model, Ec_{highcut} = cutoff energy, E_{fhighcut} = e-folding energy, T_{idiskbb} = temperature at inner regions/ radii of the keplerian disk flow, norm_{diskbb} = normalization parameter of *diskbb* model, D_{grad} = distance of the source, Θ_{grad} = disk inclination angle, M_{bhgrad} = mass of the black hole, M_{ddgrad} = optically thick flow mass accretion rate ($\dot{M}_{\text{op,thickflow}}$), hd_{grad} = spectral hardening factor (color temperature to effective temperature ratio), norm_{grad} = normalization parameter of *grad* model, E_{6.5_gaus} = iron emission line energy at 6.5 keV, sigma_{gaus} = emission line width, norm_{gaus} = normalization parameter of the Gaussian model. χ^2 (Chi-squared) = Fit/Test statistics, d.o.f = degree of freedom, R χ^2 = reduced Chi-squared, N_{H} = hydrogen column density, NhP = Null hypothesis probability.

Table 2

Best fit spectral parameter of MAXI J1535–571 using *TCAF* model.

Spectral Parameters	Epoch-A	Epoch-B	Unit
Constant factor	0.97 \pm 0.11	1.00 \pm 0.01	
N_{H}	(2.84 \pm 0.10) $\times 10^{22}$	(3.61 \pm 0.15) $\times 10^{22}$	cm ⁻²
m_{dotd}	0.621 \pm 0.010	0.794 ^{+0.113} _{-0.012}	\dot{M}_{Edd}
m_{doh}	0.586 ^{+0.007} _{-0.019}	0.572 \pm 0.02	\dot{M}_{Edd}
m_{bh}	9.520 \pm 0.03	9.621 ^{+0.162} _{-0.141}	M _⊙
Xs	42.187 ^{+1.108} _{-0.024}	39.057 ^{+2.012} _{-0.005}	r _s
R	3.98 \pm 0.06	4.002 ^{+0.001} _{-0.08}	–
norm	32.932 \pm 1.020	38.132 ^{+0.467} _{-0.501}	–
E _{6.5}	6.492 ^{+0.007} _{-0.002}	6.520 \pm 0.01	keV
E _{sigma}	0.196 \pm 0.054	0.215 ^{+0.105} _{-0.081}	keV
norm _{gaus}	1.201 \pm 0.02	1.160 \pm 0.095	–
χ^2	20.10	496.82	–
d.o.f	17	462	–
R χ^2	1.18	1.07	–
NhP	2.64 $\times 10^{-01}$	4.120 $\times 10^{-01}$	–

m_{dotd} = Keplerian flow mass accretion rate, m_{doh} = Sub-Keplerian flow (halo) mass accretion rate, R = shock compression ratio, Xs = shock location in unit of Schwarzschild radius, norm = normalization parameter of *TCAF*, E_{6.5} = iron emission line at 6.5 keV, norm_{gaus} = normalization value of Gaussian model, χ^2 (Chi-squared) = Fit/Test statistics, d.o.f = degree of freedom, R χ^2 = reduced Chi-squared, N_{H} = hydrogen column density, NhP = Null hypothesis probability.

Table 3
Pearson correlation of parameters.

Figure	parameter	Correlation coefficient (R)	P-value	Lower bound	Upper bound	Direction and strength of correlation	Is the correlation test statistically significant?
Fig. 5	Γ vs N_{bmc} - Epoch-A	0.9264	<0.0001	0.8663	0.9600	Very strong positive	yes
Fig. 6	Γ vs N_{bmc} - Epoch-B	0.8318	<0.0001	0.7526	0.8873	Very strong positive	yes
Fig. 7	$\dot{M}_{op.thinflow}$ vs $\dot{M}_{op.thickflow}$ - Epoch-A	0.6519	0.0008	0.3277	0.8387	strong positive	yes
Fig. 8	$\dot{M}_{op.thinflow}$ vs $\dot{M}_{op.thickflow}$ - Epoch-B	0.5967	<0.0001	0.4455	0.7148	strong positive	yes
Fig. 9	m_{d0th} vs m_{dotd} -Epoch-A	-0.6493	<0.0001	-0.7271	-0.5549	strong negative	yes
Fig. 10	m_{d0th} vs m_{dotd} -Epoch-B	-0.4530	<0.0001	-0.5620	-0.3285	Moderate negative	yes

Γ = photon index, N_{bmc} =normalization parameter of the bmc model, $\dot{M}_{op.thinflow}$ =optically thin flow mass accretion rate, $\dot{M}_{op.thickflow}$ =optically thick mass accretion rate, m_{d0th} =sub-Keplerian flow mass accretion rate, m_{dotd} = Keplerian mass accretion rate. The p-value <0.0001 indicates that the actual value p-value is too small for the MATLAB software to display.

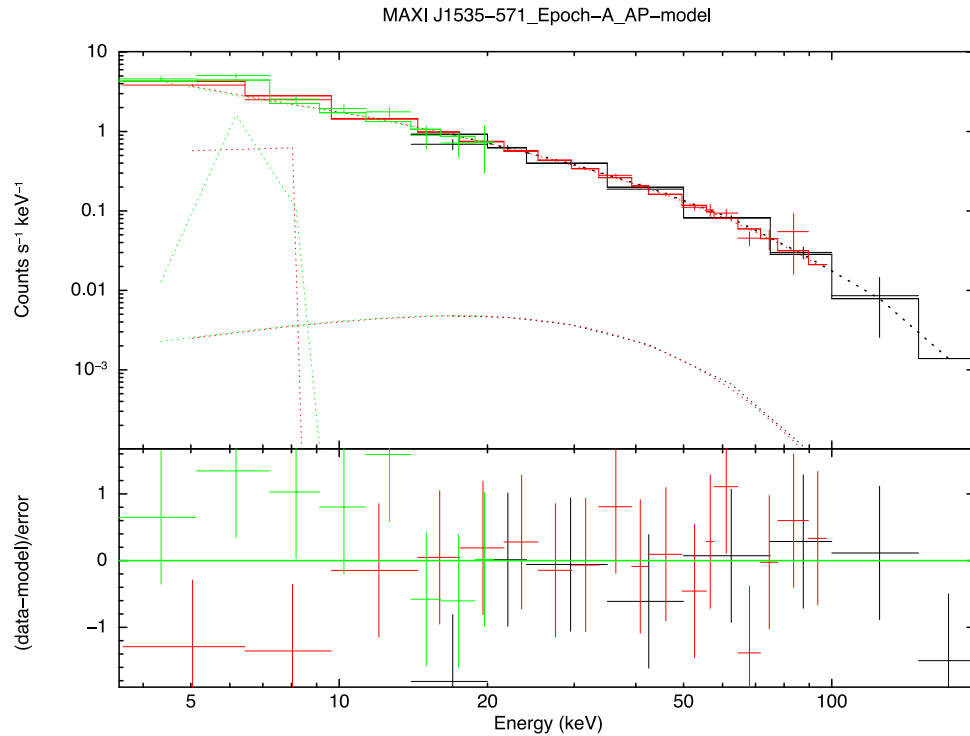


Fig. 1. X-ray spectrum of Epoch-A obtained using selected analytical and phenomenological models (AP-model). In the upper panel, the fitted data are shown by crosses; the Swift/BAT data is black, the MAXI/GSC data is green, and the NuSTAR data is red. The fitted AP-models are represented by the solid thick, broken, and curved dotted lines. The peak of the dotted curve corresponds to the 6.5 keV iron emission line. The ratio of the fitted data to the AP-models is shown in the lower panel.

Fig. 1 and 3 is the X-ray spectrum of Epoch-A and Epoch-B obtained using the AP-model respectively. Fig. 2 and 4 is the X-ray spectrum of Epoch-A and Epoch-B obtained using the TCAF model respectively. In the upper panel, the fitted data are represented by crosses; the Swift/BAT data is black, MAXI/GSC data is green, and NuSTAR data is red in Fig. 1 and Fig. 2 whereas in Fig. 3 and Fig. 4, the Swift/BAT data is black, MAXI/GSC data is red, and NuSTAR data is green. The models are represented by solid thick, broken, and curved lines. The peak of the dotted curve in Fig. 1–4 corresponds to the 6.5 keV iron emission line. The bottom panel of Fig. 1–Fig. 4, shows the ratio of the fitted data to the models. Both the AP-model and the TCAF model reproduced the data very well with a good statistical fit and a reduced Chi-squared value of ≤ 1.2 . We deem it unnecessary to include the X-ray spectra of Epoch-A and Epoch-B obtained using other models because of space. Fig. 5 and Fig. 6 show the correlation of photon index (Γ)–normalization (N_{bmc}) with error bars for Epoch-A and Epoch-B respectively. In Fig. 5, the photon index (Γ) increases in unison with the normalization parameter of the bmc and saturates at some points as N_{bmc} further increases. In Fig. 6, as Γ increases from 1.491 to 1.538, N_{bmc} increases from 0.385 to 0.3929, and an indication of saturation effect is evidenced when Γ increases from

1.538 to 1.57 and N_{bmc} = 0.3929–0.4167. Thereafter, both parameters increase in unison. Therefore, Γ and N_{bmc} are positively correlated (see Table 3). Fig. 7 and Fig. 8 show the correlation of optically thin flow mass accretion rate ($\dot{M}_{op.thinflow}$) and optically thick flow mass accretion rate ($\dot{M}_{op.thickflow}$) with error bar for Epoch-A and Epoch-B (unit; Kilogram per seconds) obtained using AP-models respectively. The $\dot{M}_{op.thinflow}$ and $\dot{M}_{op.thickflow}$ increases in unison, but as one parameter decreases the other parameter remains relatively constant and vice versa. This irregular pattern is an indication that both parameters vary. The $\dot{M}_{op.thinflow}$ and $\dot{M}_{op.thickflow}$ are positively correlated at some points and anti-correlated at some other points (see Fig. 7 & 8). Fig. 9 and Fig. 10 show the correlation of sub-Keplerian mass accretion rate (m_{d0th}) and Keplerian mass accretion rate (m_{dotd}) with the error bar for Epoch-A and Epoch-B (in Eddington mass accretion rate unit) obtained using the TCAF model respectively. While m_{d0th} decreases, m_{dotd} is relatively constant, and vice versa. These parameters are negatively or anti-correlated. The m_{d0th} and m_{dotd} have negative correlation values. Hence, both the prediction of AP-model and TCAF model are reliable because the Keplerian flow contains optically thick plasma while the sub-Keplerian flow contains optically thin plasma (See [12]).

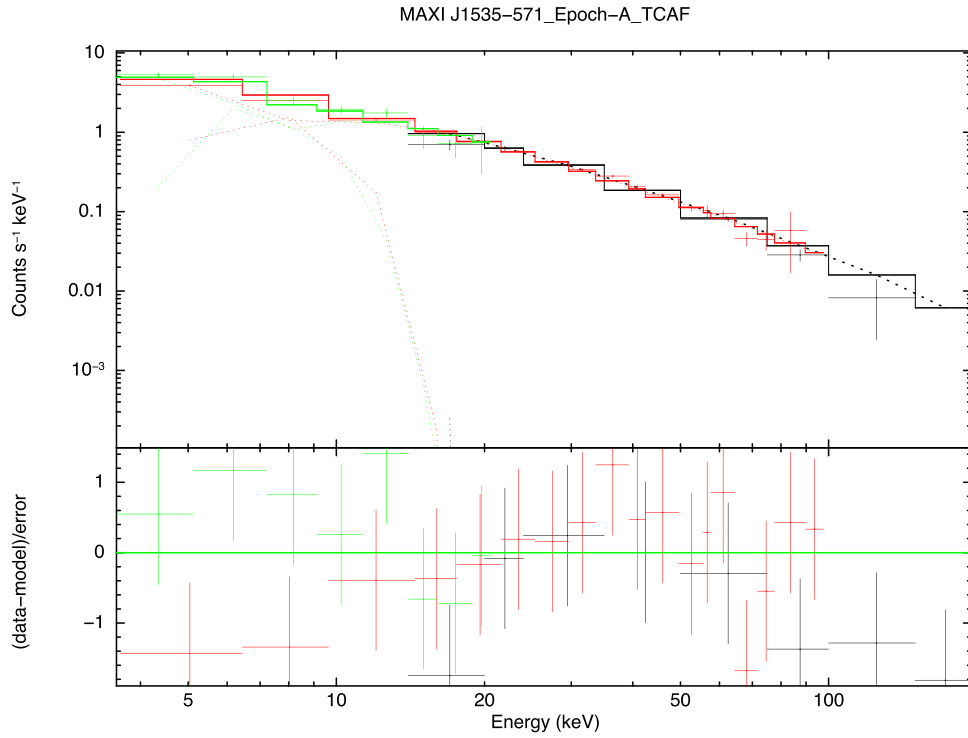


Fig. 2. X-ray spectrum of Epoch-A obtained using the *TCAF* model. In the upper panel, the fitted data are shown by crosses; the *Swift*/*BAT* data is black, *MAXI*/*GSC* data is green, and *NuSTAR* data is red, whereas the *TCAF* + *gaus* models are represented by the solid thick and dotted lines. The peak of the dotted curve corresponds to the 6.5 keV emission line. The ratio of the fitted data to the models is shown in the lower panel.

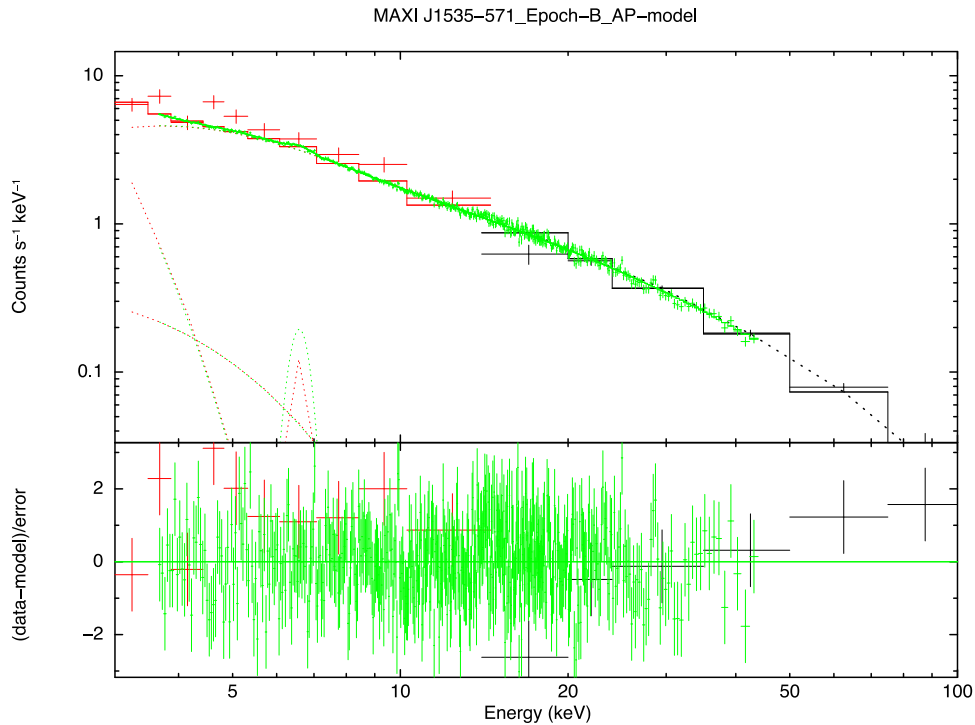


Fig. 3. X-ray spectrum of Epoch-B obtained using selected analytical and phenomenological models (AP-models). In the upper panel, the fitted data are shown by crosses; the *Swift*/*BAT* data is black, the *MAXI*/*GSC* data is red, and the *NuSTAR* data is green. The fitted AP-model are represented by solid thick, broken, and curved lines. The peak of the dotted curve corresponds to the iron emission line at 6.5 keV. The ratio of the fitted data to the AP-models is shown in the lower panel.

So, the AP-model and physical model (*TCAF*) explain the components of the accretion flow and their mass accretion rates with different perceptions, but with the same context. The context is that the accretion flow consists of two components. Moreover, hard X-rays are produced

during the hard spectral state when the outside ISCO of the accretion disk is truncated and inefficient radiative hot plasma thermally comptonized the soft photons (truncated disk model; AP-model). In the same vein, *TCAF* presumes that hard X-rays are produced when the soft

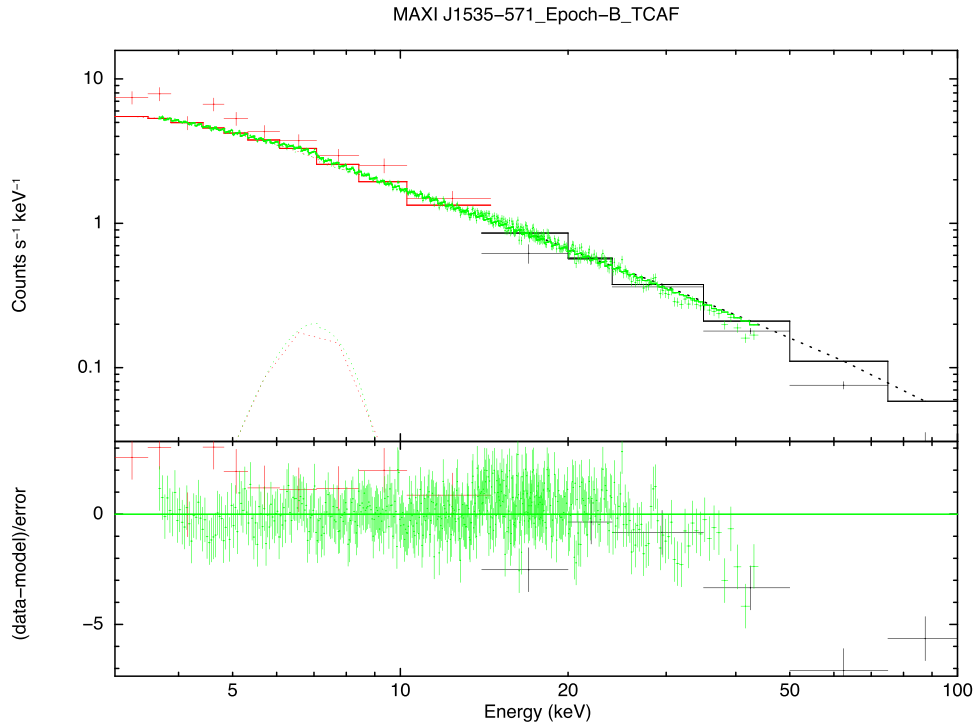


Fig. 4. X-ray spectrum of Epoch-B obtained using the *TCAF* model. In the upper panel, the fitted data are shown by crosses; the *Swift/BAT* data is black, *MAXI/GSC* data is red, and *NuSTAR* data is green, whereas the fitted *TCAF+gaus* models is represented by the solid thick and dotted lines. The broken line parabolic curve in the upper panel is the Gaussian model which is peak corresponds to the 6.5 keV emission line. The ratio of the fitted data to the models is shown in the lower panel.

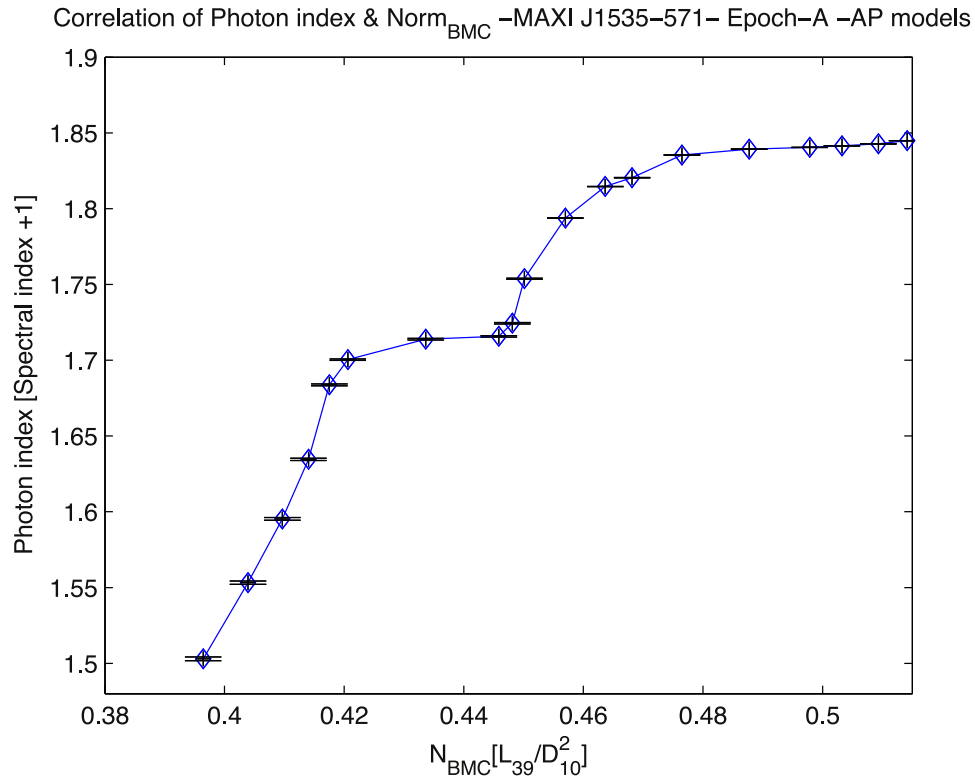


Fig. 5. Correlation between photon index and Normalization parameter of *Bmc* model for Epoch-A. The data is diamond(blue) and the error associated with each data is the black solid dashed line.

photons from the Keplerian region are conveyed through magnetic activities to the sub-Keplerian region where they are inverse-comptonize by hot electrons. The *TCAF* assumes CENBOL while the truncated disk

model (AP-model) assumed ISCO. Therefore, when the prediction of one model is correct, the other is reliable. The combination of these models reveals the dynamical behavior of accretion flow and its components

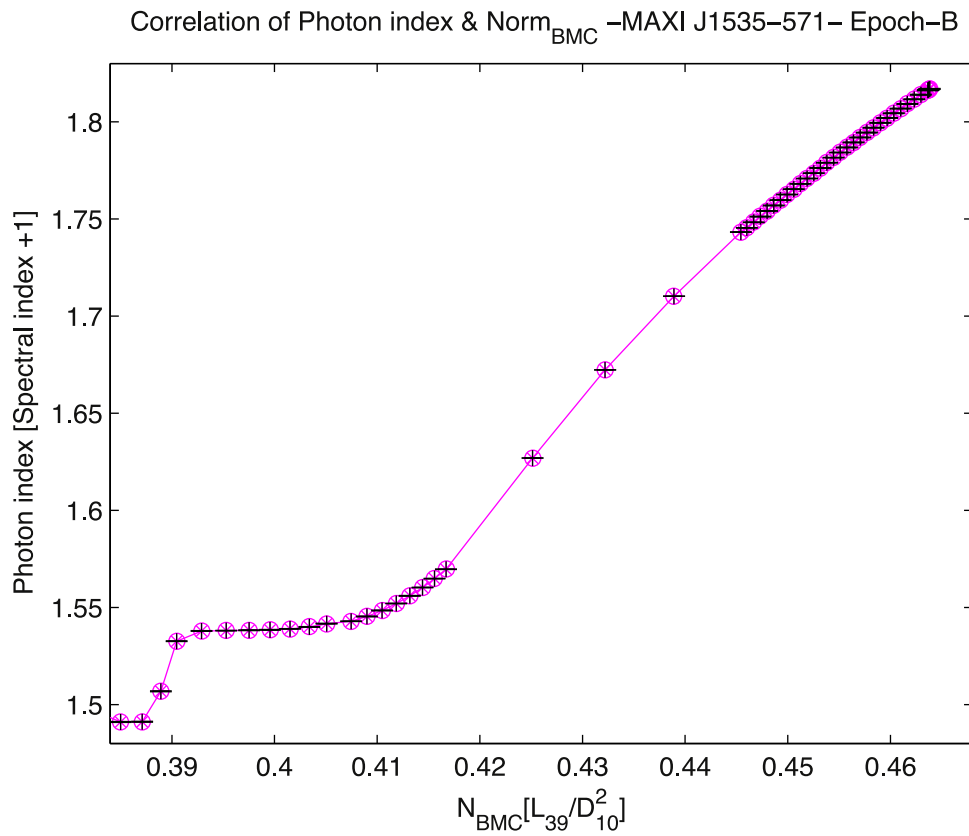


Fig. 6. Correlation between photon index and Normalization parameter of *Bmc* model for Epoch-B. The data is circled asterisk(magenta) and the error associated with each data is the black cross.

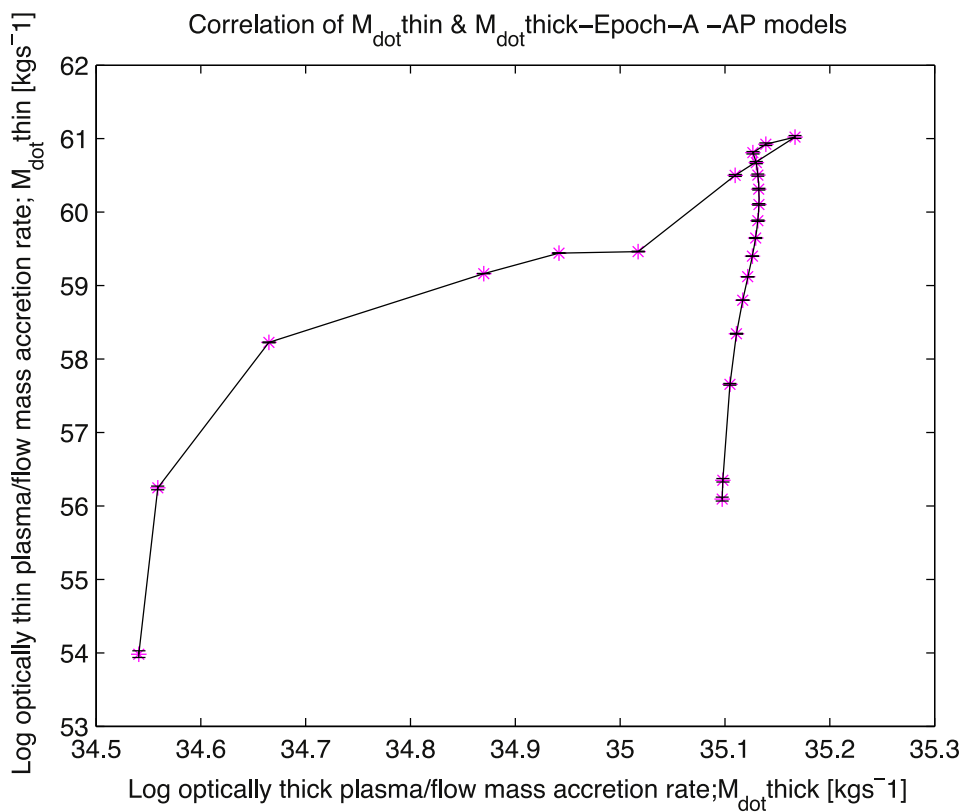


Fig. 7. Correlation between optically thin and optically thick mass accretion rates of Epoch-A *AP*-model. The data is an asterisk(*; magenta) and the error associated with each data is the black solid dash line.

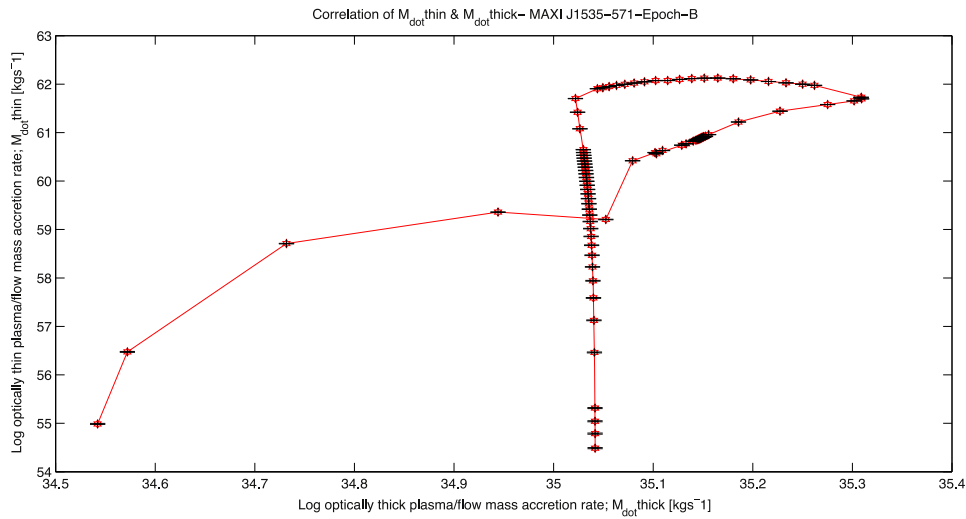


Fig. 8. Correlation between optically thin and optically thick mass accretion rates of Epoch-B_AP-model. The data is the hexagram(red), and the error associated with each data is the black cross.

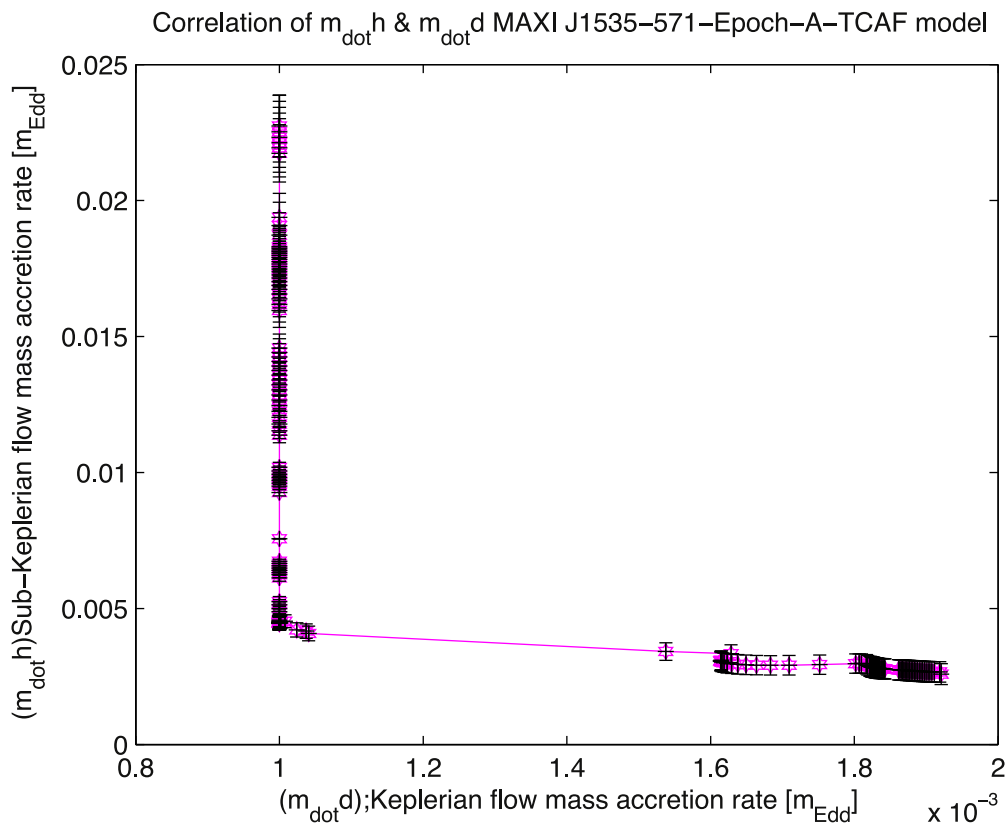


Fig. 9. Correlation between sub-Keplerian and Keplerian mass accretion rates of Epoch-A_TCAF model. The data is the asterisk (*; magenta), and the error associated with each data is the black solid dash line.

(driven by activities/viscosity) around the black hole as the outburst progresses. Hence, components of the accretion flow rates seem to vary and positively or negatively correlate to one another, fluctuate, and saturate at different phases as the outburst progresses. Fig. 11 and Fig. 12 show the contour plot of the $m_{\dot{d}}$ and $m_{\dot{h}}$ at three different intervals for Epoch-A and Epoch-B respectively. These contour plots were obtained by linear “steppar” techniques to simultaneously run different iterations of $m_{\dot{d}}$ and $m_{\dot{h}}$ concurrently. This is why the value of $m_{\dot{d}}$ and $m_{\dot{h}}$ in the vertical and horizontal axes of Fig. 11 and Fig. 12 is different from what was inferred in Table 2. An inspection

of Fig. 11 and Fig. 12 shows a “zig-zag” pattern though it is more elaborate in Fig. 11. This “zig-zag” pattern shows a strong correlation between $m_{\dot{d}}$ and $m_{\dot{h}}$. Moreover, the TCAF model-fitted spectra give the probable mass of the black hole in the range of $\sim 9.5\text{--}9.62 M_{\odot}$ with an average value of $9.57 M_{\odot}$ whereas the AP-model gives probable mass of the black hole in the range of $9.6\text{--}10 M_{\odot}$ with an average value of $9.9 M_{\odot}$. This agrees with the previous studies on BHCs [63–65]. However, there might be uncertainty in the model-fitted mass of the black hole due to measurements. It is worth noting that there are “data gaps” in Fig. 6–Fig. 10 which we believe are associated with instruments or there

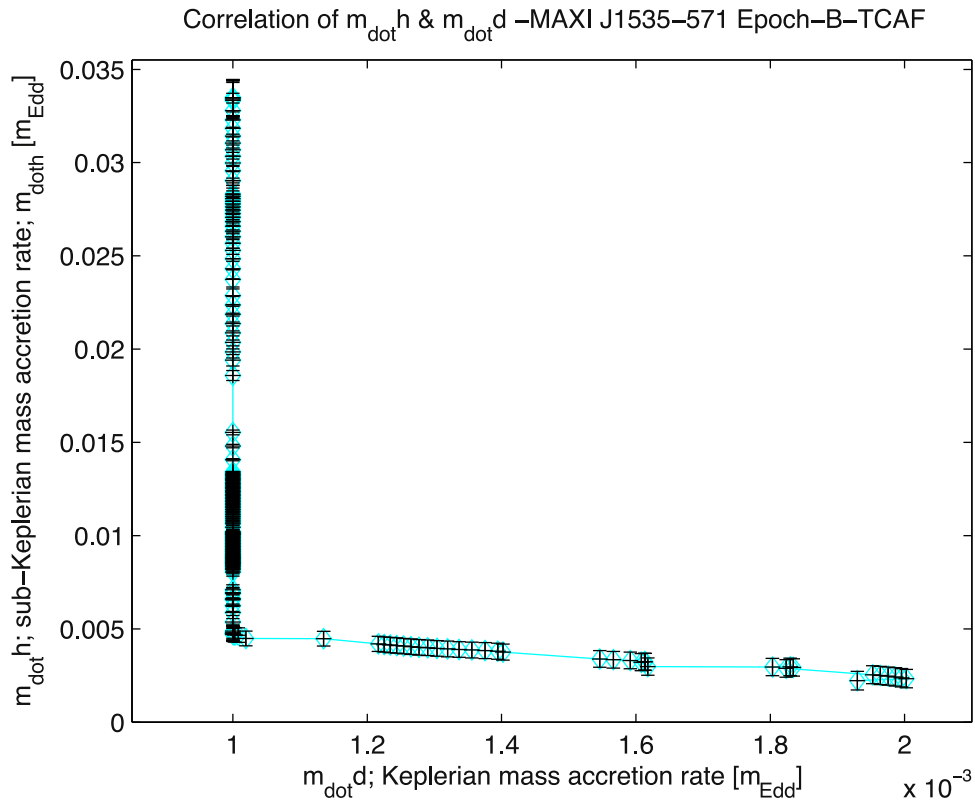


Fig. 10. Correlation between sub-Keplerian and Keplerian mass accretion rates of Epoch-B_TCAF model. The data is circled (cyan) and the error associated with each data is black cross.

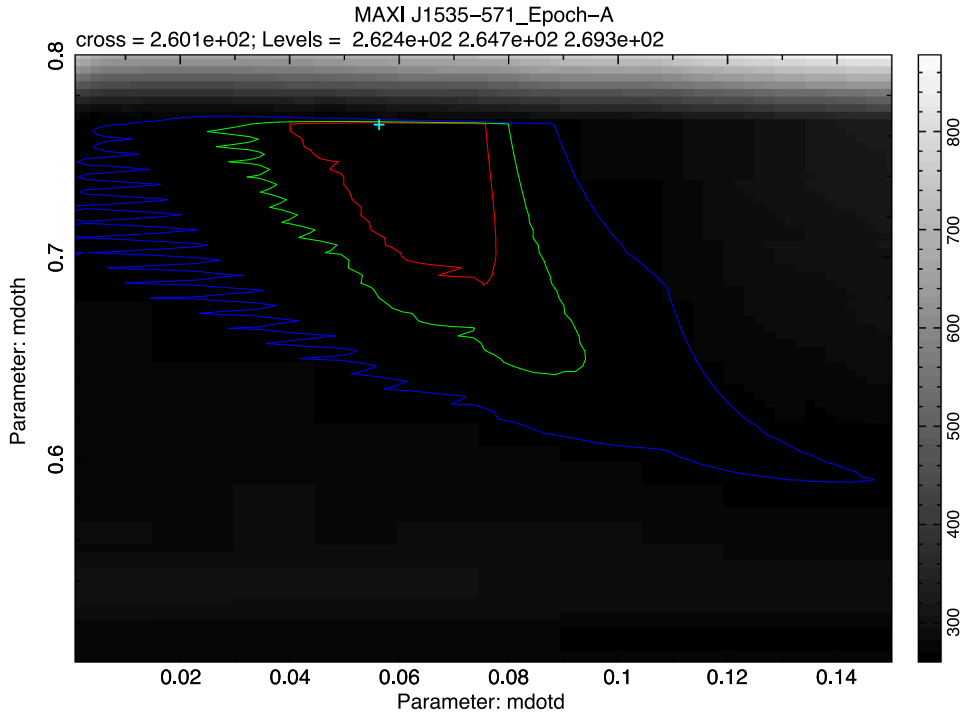


Fig. 11. Contour plot of $m_{\dot{d}h}$ and $m_{\dot{d}d}$ Epoch-A at different confidence levels. The plus sign “+” represents the minimum fit-statistic (2.601×10^2). The second and third fit-statistic level is 2.647×10^2 , and 2.693×10^2 respectively. The color bar on the right hand is the delta-fit statistic.

is an obscuration in the observation line of sight and/or lower statistics from the spectra data.

4. Discussion and conclusion

We can deduce from our spectral analysis and results that MAXI J1535–571 accretion flow components are distinct and are represented

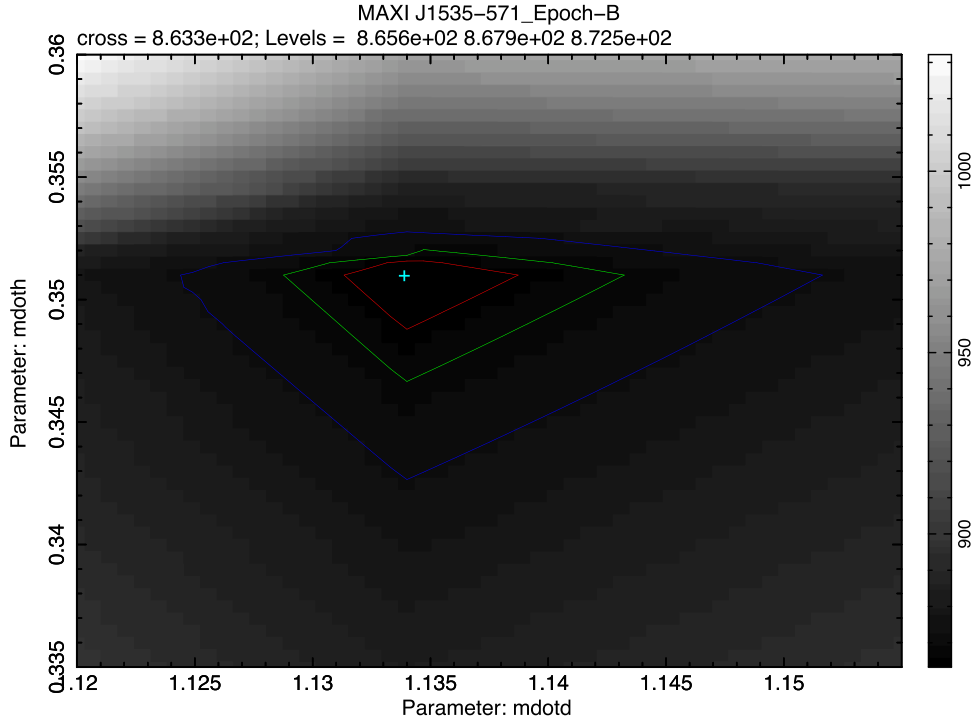


Fig. 12. Contour plot of \dot{m}_{oth} and \dot{m}_{od} Epoch-B at different confidence levels. The plus sign “+” represents the minimum fit-statistic (8.633×10^2). The second and third fit statistic level is 8.656×10^2 , and 8.725×10^2 respectively. The color bar on the right hand is the delta-fit statistic.

by the optically thick flow/plasma and optically thin flow/plasma based on the adopted AP-model (XSPEC; [10,11,33,48,49]). Also, we can deduce from our spectral analysis and results that the MAXI J1535-571 accretion flow consists of Keplerian flow and sub-Keplerian flow components based on the adopted TCAF model [66]. The sub-Keplerian flow contains optically thin plasma while the Keplerian flow contains optically thick plasma [12]. These components of the accretion flow vary, coexist with one another, and explain the power law and multi-color X-radiations of MAXI J1535-571. The optically thin flow is geometrically thick whereas the optically thick flow is geometrically thin [11]. The 6.5 keV iron emission line, reflection fraction of 4.65, and lamp-post height of 6.251 (GM/c²) are an indication of reflection components of X-radiations [62]. The variations/fluctuations of components of the accretion flow rates significantly contribute to the hard X-ray emissions via thermal and inverse comptonization processes and decipher the energy spectral index [11,12,54,67]. The best-fit photon index in the range of 2.0-2.2 indicates that MAXI J1535-571 is in the hard-intermediate state (see; [43,44]). We were able to obtain Γ - N_{bmc} track of MAXI J1535-571 that depicts the photon index saturation effect as has been reported by Nakahira et al. [43] which is similar to the same phenomena seen in other Galactic sources [21,33,68,69]. The saturation effect is an indication of converging flow [16,49] which begins when the cooling process gradually douses the heating [70]. This suggests that the saturation effect in the photon index as N_{bmc} increases is tied to variations/fluctuations of components of the accretion flow rates. We were able to obtain the variations in optically thick and optically thin mass accretion flow rates as; $\dot{M}_{\text{op.thickflow}} = 34.5408 - 35.1669$ and $\dot{M}_{\text{op.thinflow}} = 53.9815 - 61.0229$ for Epoch-A, $\dot{M}_{\text{op.thickflow}} = 34.5421 - 35.309$ and $\dot{M}_{\text{op.thinflow}} = 54.9874 - 62.1253$ for Epoch-B (AP-models; all units in $\log \text{kg s}^{-1}$) respectively. The value of $\dot{M}_{\text{op.thickflow}}$ inferred in Table 1 is obtained after “steppar” techniques. The optically thin and optically thick mass accretion rates vary in unison at some points, but when the optically thin mass accretion rate is gradually decreasing, the optically thick mass accretion rate is relatively constant and vice versa (see Fig. 7 and 8). This is a result of the truncation of the outer region of the innermost stable circular orbit and the comptonization of soft photons by

high-temperature electrons [10,11]. The $\dot{M}_{\text{op.thickflow}}$ and $\dot{M}_{\text{op.thinflow}}$ are positively correlated and anti-correlated at some points. Also, we were able to obtain the variations in Keplerian and sub-Keplerian mass accretion rates directly from the TCAF model as; $\dot{m}_{\text{dotd}} = 0.001 - 0.00192093$ and $\dot{m}_{\text{doh}} = 0.00258958 - 0.0227373$ for Epoch-A, $\dot{m}_{\text{dotd}} = 0.001 - 0.00200254$ and $\dot{m}_{\text{doh}} = 0.00221824 - 0.03346$ for Epoch-B (all units in \log Eddington limit) respectively.

When the sub-Keplerian mass accretion rate is decreasing, the Keplerian mass accretion rate is relatively constant and when the sub-Keplerian mass accretion rate is relatively constant, the Keplerian mass accretion rate is increasing (see Fig. 9 and 10). This irregular pattern in variations of sub-Keplerian and Keplerian mass accretion rates suggests that both parameters vary. This agrees with the results of Nandi et al. [71] who observed similar phenomena during the hard or hard-intermediate spectral state of BHCs. Hence, \dot{m}_{doh} and \dot{m}_{dotd} are anti-correlated and their correlation is statistically significant (see; Table 3). It is worth noting that the value of \dot{m}_{dotd} and \dot{m}_{doh} plotted in Fig. 9 and Fig. 10 were obtained using model-fitted values while the values of \dot{m}_{dotd} and \dot{m}_{doh} inferred in Table 2 were obtained from additional technique. The \dot{m}_{dotd} and \dot{m}_{doh} were “steppar” separately one at a time and their values inferred in Table 2 were obtained. Moreover, we were able to obtain elaborate variations/fluctuations of \dot{m}_{doh} and \dot{m}_{dotd} at three different confidence intervals. The “zig-zag” pattern depicts that \dot{m}_{doh} and \dot{m}_{dotd} are strongly correlated (see Fig. 11 and 12). The value of \dot{m}_{dotd} and \dot{m}_{doh} inferred in Table 2 indicates that the accretion rate ratio (ARR; $\dot{m}_{\text{doh}}/\dot{m}_{\text{dotd}}$) in each Epoch-A and Epoch-B spectrum is 0.943 and 0.720 respectively. This implies that the ARR decreases during the rising outburst phases [65,71,72]. The decrease in the accretion rate ratio (ARR) indicates that the Keplerian flow gradually increases and interacts at varying distances with the sub-Keplerian flow as their mass accretion rate change [12]. This strongly affects the hardness of X-ray emissions/flux variability [43,44,66,71,72]. This suggests that the variations/fluctuations of the components of the accretion rates (\dot{m}_{doh} & \dot{m}_{dotd}) initiate, mediate, and regulate the fractions of both the hard and soft components of the X-ray radiations [12,19,34,65,73]. Therefore, components of the accretion

flow rates vary/fluctuate and their variations/fluctuations suggest that the accretion flow is dynamic. Hence, $\dot{m}_{\text{dot}h}$ and $\dot{m}_{\text{dot}d}$ seem to be the intrinsic properties/parameters that regulate the dynamics, structure, and geometry of the accretion flow.

CRedit authorship contribution statement

Ambrose C. Eze: Writing – original draft, Project administration, Methodology, Formal analysis, Conceptualization, Investigation. **Romanus N.C. Eze:** Writing – review & editing, Supervision, Project administration, Investigation, Formal analysis, Data curation, Conceptualization, Validation. **Augustine E. Chukwude:** Writing – review & editing, Supervision, Project administration, Investigation. **Fidelis O. Madu:** Conceptualization, Writing – original draft.

Declaration of competing interest

The authors declare that they have no known competing financial interests or personal relationships that could have appeared to influence the work reported in this paper.

Acknowledgment

We are grateful to the Japan Society for the Promotion of Science (JSPS) for sponsoring RNCE, at Ehime University, 2–5, Bunkyocho, Matsuyama, Ehime 790–8577, Japan, under JSPS Invitation Fellow (short term) where this project was initiated and *Swift/BAT*, *MAXI/GSC*, and *NuSTAR* observation team for providing data and relevant files used in the analysis presented here. We also acknowledge the useful discussions and assistance of Megumi Shidatsu in the analysis of data used in the paper. Also, ACE is grateful for the financial assistance of the African Astronomical Society (AFAS) towards this research. Opinions expressed and conclusions arrived at are those of the author and are not necessarily to be attributed to AfAS. www.africanastronomicalsociety.org. We are also grateful to Dipak Debnath of the Institute of Astronomy, Space and Earth Science, India for providing us the *TCAF* model and his guidance and assistance.

Data availability

<https://heasarc.gsfc.nasa.gov/docs/archive.htm> (http://maxi.riken.jp/mxondem/)

References

- [1] S.A. Balbus, J.F. Hawley, A powerful local shear instabilities in weakly magnized disk. I-linear analysis, II-Nonlinear evolution, *ApJ* 376 (1991) 214.
- [2] S.A. Balbus, J.F. Hawley, A powerful local shear instabilities in weakly magnized disk IV; Nonaxisymmetric perturbations, *ApJ* 400 (1992) 610–621.
- [3] S.A. Balbus, J.F. Hawley, Instability, turbulence, and enhanced transport in accretion disks, *Rev. of Mod. Phys.* 70 (1998), <https://doi.org/10.1103/RevModPhys.70.1>.
- [4] R.D. Blandford, D.G. Payne, Hydromagnetic flows from accretion discs and production of radio jets, *MNRAS* 199 (1982) 883–903.
- [5] K. Ebisawa, L. Titarchuk, S.K. Chakrabarti, On the spectral slopes of hard x-ray emission from black hole candidates, *PASJ* 48 (1996) 59–65.
- [6] D. Proga, Numerical simulation of mass outflows driven from accretion disks by radiation and magnetic forces, *ApJ* 585 (2003) 406–417.
- [7] T.M. Belloni, States and Transitions in Black-Hole Binaries, *Lect. Notes Phys.* 794 (2009) 53–84, <https://doi.org/10.1007/978-3-540-76937-83>. <http://arxiv.org/abs/0909.2474v1>.
- [8] M.C. Baglio, D.M. Russell, P. Casella, et al., A wildly flickering jet in the black hole X-ray binary MAXI J1535–571, *ApJ* 867 (2018) 114, <https://doi.org/10.3847/1538-4357/aac532>.
- [9] R. Blandford, Black Holes as Cosmic Dynamos. *Proceedings of Science*, 2019. <https://pos.sissa.it/>.
- [10] A. Kubota, K. Makishima, The three spectral regimes found in the stellar blackhole XTE J1550–564 in its high/soft state, *ApJ* 601 (2004) 428–438.
- [11] Done, C., Gierliński, M., & Kubota, A., (2007), Modelling the behaviour of accretion flows in X-ray binaries. <http://arxiv.org/abs/0708.0148v1>.
- [12] S.K. Chakrabarti, L.G. Titarchuk, Spectral properties of accretion disks around galactic & extragalactic black holes, *ApJ*, 455 (1995) 623.
- [13] S.K. Chakrabarti, S.G. Manickam, Correlation among quasi-periodic oscillation frequencies and quiescent-state duration in black hole candidate GRS1915+ 105, *ApJ* 531 (1) (2000) L41.
- [14] Galeev, Rosner, Vaiana, Structured coronae of accretion disks, *ApJ* 229 (1979) 318–326.
- [15] L. Titarchuk, A. Mastichiadis, N.D. Kylafis., Spherical accretion onto neutron stars and black holes (1996). *arXiv preprint astro-ph/9611084*.
- [16] L. Titarchuk, A. Mastichiadis, N.D. Kylafis, X-ray spectral formation in a converging fluid flow: spherical accretion into blackholes, *ApJ* 487 (1997) 834–846.
- [17] A.A. Esin, R. Narayan, W. Cui, J.E. Grove, S.N. Zhang, Spectral transitions in Cygnus X-1 and other blackhole X-ray binaries, *ApJ*, 505 (1998) 854–868.
- [18] Chakrabarti, S.K. (1999). Estimation and effects of the mass outflow rate from shock compressed flow around compact objects. *arXiv preprint astro-ph/9910014*.
- [19] K. Ebisawa, F. Makino, K. Mitsuda, T. Belloni, A.P. Cowley, P.C. Schmidtke, A. Treves, Spectral variations of LMC X-3 observed with GINGA, *ApJ* 403 (1993) 684–689.
- [20] K. Ebisawa, M. Ogawa, T. Aoki, T. Dotani, M. Takizawa, Y. Tanaka, K. Yoshida, S. Miyamoto, et al., Spectral evolution of the bright X-ray Nova GS 1124–68 (Nova Muscae 1991) observed with Ginga, *PASJ* 46 (1994) 375–394.
- [21] P. Laurent, L. Titarchuk, The converging inflow spectrum is an intrinsic signature for a black hole: monte carlo simulations of comptonization on free-falling electrons, *ApJ* 511 (1) (1999) 289.
- [22] J. Homan, T. Belloni, The evolution of Blackhole States, *Astroph. & Space Science* 30 (2005) 107–117, <https://doi.org/10.1007/s10509-005-1197-4>, 2005.
- [23] R.A. Remillard, J.E. McClintock, X-ray Properties of Black-Hole Binaries, *A&A* 44 (2006) 49.
- [24] Belloni, T.M., (2006), Blackhole transient: from QPOs to relativistic jets. <http://arxiv.org/abs/astro-ph/0507556v2>.
- [25] T.M. Belloni, S.E. Motta, T. Muñoz-Darias, Black hole transients, *Bull. Astr. Soc. India* 39 (2011) 1–20.
- [26] A.A. Esin, J.E. McClintock, R. Narayan, Advection-dominated accretion & the spectral states of black hole X-Ray Binaries: application to Nova MUSCAE1991, *ApJ*, 489 (1997) 865–889.
- [27] A. Kubota, Y. Tanaka, K. Makishima, Y. Ueda, T. Dotani, H. Inoue, K. Yamaoka, Evidence for a black hole in the X-Ray Transient GRS 1009-45, *PASJ* 50 (1998) 667–673.
- [28] M. Gierliniński, A.A. Zdziarski, J. Poutanen, P.S. Coppi, K. Ebisawa, W.N. Johnson, Radiation mechanisms and geometry of Cygnus X-1 in the soft state, *MNRAS* 309 (1999) 496–512.
- [29] R. Narayan, J.E. McClintock, I. Yi, A New model for black hole soft X-ray transients in quiescence, *ApJ*, 457 (1995) 821.
- [30] C.R. Shrader, L. Titarchuk, Mass determination of black holes in LMC X-1 and Nova Muscae 1991 from their high-energy spectra, *ApJ* 521 (1999) L121–L124.
- [31] X. Cao, A.A. Zdziarski, Jets in the soft state in Cyg X-3 caused by advection of the donor magnetic field and unification with low-mass X-ray binaries, *MNRAS* 000 (2020) 1–9.
- [32] L. Titarchuk, T. Zannias, The extended power law as an intrinsic signature for a black hole, *ApJ* 493 (2) (1998) 863.
- [33] L. Titarchuk, E. Seifina, A. Chekhtman, O. Indira, Spectral index – mass accretion rate correlation and evaluation of black hole masses in AGNs 3C 454.3 and M 87, *A&A* 633 (2020) A73, <https://doi.org/10.1051/0004-6361/201935576>.
- [34] Shaposhnikov, N., & Titarchuk, L., (2009), Determination of black hole masses in galactic black hole binaries using scaling of spectral and variability characteristics. <http://arxiv.org/abs/0902.2852v1>.
- [35] H. Negoro, T. Kawase, M. Sugizaki, et al., Further brightening of the X-ray transient MAXI J1535–571, suggesting the presence of a black hole, *Astrono. Teleg.* (2017) 10708.
- [36] M. Matsuoka, K. Kawasaki, S. Ueno, et al., The MAXI mission on the ISS: science and instruments for monitoring All-Sky X-Ray Images, *PASJ* 61 (2009) 999–1010.
- [37] J.A. Kennea, P.A. Evans, A.P. Beardmore, et al., *Astrono. Teleg.* (2017) 10700.
- [38] Xu, Y.A., Harrison F.A., Garcia, J.A., (2018), Reflection Spectra of the blackhole candidate MAXI J1535–571 in the hard state observed by NUSTAR. <https://arxiv.org/abs/1711.01346v2>.
- [39] M. Shidatsu, S. Nakahira, H. Negoro, et al., MAXI/GSC observations indicate further softening of MAXI J1535–571 toward the high/soft state, *Astrono. Teleg.* (2017) 10761.
- [40] A.J. Tetarenko, T.D. Russell, J.C.A. Miller-Jones, G.R. Sivakoff, Extremely Bright Radio and (Sub-)Millimetre Detections of MAXI J1535–571, *Astrono. Teleg.* (2017) 10745.
- [41] T.D. Russell, J.C.A. Miller-Jones, G.R. Sivakoff, A.J. Tetarenko, Xrb Jacpot, Collaboration, ATCA radio detection of MAXI J1535–571 indicates it is a strong black hole X-ray binary candidate, *Astrono. Teleg.* (2017) 10711.
- [42] J. Chauhan, J.C.A. Miller-Jones, G.E. Anderson, et al., An H i absorption distance to the black hole candidate X-ray binary MAXI J1535–571, *MNRAS* 000 (2019) 1–5. <https://www.arXiv:1905.08497v2>.
- [43] Nakahira, S., Shidatsu, M., Makishima, K., et al., (2018), Discovery and state transitions of the new Galactic black hole candidate MAXI J1535 – 571. <https://arxiv.org/abs/1804.00800v2>.
- [44] L. Tao, Y. Chen, C. Güngör, Y. Huang, F. Lu, J. Qu, S. Zhang, Swift observations of the bright uncatalogued X-ray transient MAXI J1535–571, *Mon. Not. R. Astron. Soc.* 480 (4) (2018) 4443–4454.
- [45] Mereminskiy, I.A., Grebenev, S.A., Prosvetov, A.V., & Semena, A.N., (2018), Low frequency quasi-periodic oscillations in the x-ray nova maxi j1535-571 at the initial stage of its 2017 outburst. <http://arxiv.org/abs/1806.06025v1>.

- [46] V.A. Cúneo, K. Alabarta, L. Zhang, D. Altamirano, M.E. Mendez, M. Armas Padilla, A. Basak, A NICER look at the state transitions of the black hole candidate MAXI J1535– 571 during its reflares, *MNRAS* 496 (2) (2020) 1001–1012.
- [47] R.J.H. Dunn, R.P. Fender, E.G. Körding, C. Cabanac, T. Belloni, Studying the X-ray hysteresis in GX 339– 4: the disc and iron line over one decade, *MNRAS* 387 (2) (2008) 545–563.
- [48] K. Borozdin, M. Revnivtsev, S. Trudolyubov, C. Shrader, L. Titarchuk, Do the spectra of soft X-ray transients reveal bulk-motion inflow phenomenon? *ApJ* 517 (1999) 67–380.
- [49] Titarchuk, L., & Seifina, E., (2016), Scaling of the photon index vs mass accretion rate correlation and estimate of black hole mass in M101 ULX-1. <http://de.arxiv.org/abs/1510.06978v1>.
- [50] F. Vignarca, S. Migliari, T. Belloni, D. Psaltis, M Van Der Klis, Tracing the power-law component in the energy spectrum of black hole candidates as a function of the QPO frequency, *A & A* 397 (2) (2002) 729–738.
- [51] L. Titarchuk, N. Shaposhnikov, V. Arefiev, Power spectra of black holes and neutron stars as a probe of hydrodynamic structure of the source: diffusion theory and its application to Cygnus X-1 and Cygnus X-2 X-ray observations, *Astrophys. J.* 660 (1) (2007) 556.
- [52] K. Mikashima, Y. Maejima, K. Mitsuda, H.V. Bradt, R.A. Remillard, I.R. Tuohy, R. Hoshi, M. Nakagawa, Simultaneous X-ray and Optical Observations of GX 339-4 in an X-ray high state, *ApJ* 308 (1986) 635–643.
- [53] T. Shimura, F. Takahara, On the spectral hardening factor of the X-ray emission from accretion disks in blackhole candidates, *ApJ* 445 (1995) 780–788.
- [54] M. Shidatsu, Y. Ueda, S. Yamada, et al., Spectral and Timing properties of the blackhole X-ray binary H1734 -322 in the low/hard state studied with Suzaku, *ApJ*, 789 (2014) 100, <https://doi.org/10.1088/0004-637X/789/2/100>.
- [55] S.K. Chakrabarti, S. Mandal, The spectral properties of shocked Two-component accretion flows in the presence of synchrotron emission, *ApJ* 642 (2006) L49–L52.
- [56] S.K. Chakrabarti, D. Debnath, A. Nandi, P.S. Pal, Evolution of the quasi-periodic oscillation frequency in GRO J1655-40 – Implications for accretion disk dynamics, *A&A* 489 (2008) L41–L44, <https://doi.org/10.1051/0004-6361:200810136>.
- [57] Debnath, Chakrabarti, Mondal, Implementation of two component advective flow solution inXSPEC, *MNRAS* 000 (2014), 000–000.
- [58] J. Wilms, A. Allen, R. McCray, On the absorption of X-rays in the interstellar medium, *ApJ* 542 (2) (2000) 914.
- [59] K. Mitsuda, et al., Energy spectra of low-mass binary X-ray sources observed from TENMA, *PASJ* 36 (1984) 741–759.
- [60] K. Ebisawa, K. Mitsuda, T. Hanawa, Application of a general relativistic accretion disk model to LMC X-1, LMC X-3, X1608-522, & X1636-536, *ApJ* 367 (1991) 213–220.
- [61] T. Yaqoob, X-ray transmission in cold matter: nonrelativistic corrections for compton scattering, *Astrophys. J.* 479 (1) (1997) 184.
- [62] T. Dauser, J. García, M.L. Parker, A.C. Fabian, J. Wilms, The role of the reflection fraction in constraining black hole spin, *MNRAS: Letters* 444 (1) (2014) L100–L104, <https://doi.org/10.1093/mnrasl/slu125>.
- [63] A.A. Molla, D. Debnath, S.K. Chakrabarti, S. Mondal, A. Jana, Estimation of the mass of the black hole candidate MAXI J1659– 152 using TCAF and POS models, *MNRAS* 460 (3) (2016) 3163–3169.
- [64] D. Chatterjee, D. Debnath, S.K. Chakrabarti, S. Mondal, A. Jana, Accretion flow properties of MAXI J1543–564 during 2011 outburst from the TCAF solution, *Astrophys. J.* 827 (1) (2016) 88.
- [65] J.R. Shang, D. Debnath, D. Chatterjee, A. Jana, S.K. Chakrabarti, H.K. Chang, C. L. Chiu, Evolution of X-ray Properties of MAXI J1535-571: analysis with the TCAF Solution, *Astrophys. J.* 875 (1) (2019) 4.
- [66] A. Banerjee, A. Bhattacharjee, D. Debnath, S.K. Chakrabarti, Spectral analysis of γ class data of GRS 1915+105 using TCAF solution, *RAA* Vol. 20 (12) (2020) 208, <https://doi.org/10.1088/1674-4527/20/12/208>, 202010pp.
- [67] Debnath, D., Mondal, S., & Chakrabarti, S.K., (2015), Characterization of GX 339-4 outburst of 2010 –11: analysis by XSPEC using Two-Component advective model. <https://arxiv.org/abs/1306.3745v3>.
- [68] L. Titarchuk, N. Shaposhnikov, E. Seifina, Discovery of photon index saturation in the black hole binaries, in: AIP Conference Proceedings 1205, American Institute of Physics, 2010, pp. 168–176.
- [69] E. Seifina, L. Titarchuk, On the Constancy of the Photon Index of X-ray spectra of 4U 1728-34 through all spectral states, *Astrophys. J.* 738 (2) (2011) 128.
- [70] R.D. Blandford, D.G. Payne, Compton scattering in a converging fluid flow–II. Radiation-dominated shock, *MNRAS* 194 (4) (1981) 1041–1055.
- [71] A. Nandi, S. Mandal, H. Sreehari, D. Radhika, S. Das, I. Chattopadhyay, N. Iyer, V. K. Agrawal, R. Aktar, Accretion flow dynamics during 1999 outburst of XTEJ1859 +226—Modeling of broadband spectra and constraining the source mass, *Astrophys. Space Sci.* 363 (2018) 90, <https://doi.org/10.1007/s10509-018-3314-1>.
- [72] A. Nandi, D. Debnath, S. Mandal, S.K. Chakrabarti, Accretion flow dynamics during the evolution of timing and spectral properties of GX 339-4 during its 2010–11 outburst, *A & A* 542 (2012) A56.
- [73] S. Mondal, S.K. Chakrabarti, Implications on accretion flow dynamics from spectral study of Swift J1357.2-0933, *MNRAS* 000 (2019), 000–000, <https://arxiv.org/abs/1811.09502v1>.